JACS
JOURNAL OF THE AMERICAN CHEMICAL SOCIETY

Article

pubs.acs.org/JACS

Phosphoryl Transfers of the Phospholipase D Superfamily: A Quantum Mechanical Theoretical Study

Nathan J. DeYonker and Charles Edwin Webster*

The Department of Chemistry, The University of Memphis, 213 Smith Chemistry Building, Memphis, Tennessee 38152-3550, United States

Supporting Information

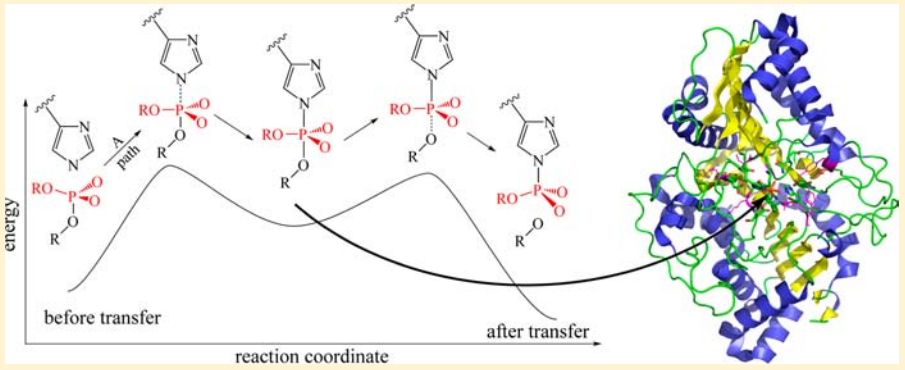

ABSTRACT: The HKD-containing Phospholipase D superfamily catalyzes the cleavage of the headgroup of phosphatidylcholine to produce phosphatidic acid and choline. The mechanism of this cleavage process is studied theoretically. The geometric basis of our models is the X-ray crystal structure of the five-coordinate phosphohistidine intermediate from *Streptomyces sp*. Strain PMF (PDB Code = 1V0Y). Hybrid ONIOM QM:QM methodology with Density Functional Theory (DFT) and semiempirical PM6 (DFT:PM6) is used to acquire thermodynamic and kinetic data for the initial phosphoryl transfer, subsequent hydrolysis, and finally, the formation of the experimentally observed ″dead-end″ phosphohistidine product (PDB Code = 1V0W). The model contains nineteen amino acid residues (including the two highly conserved HKD-motifs), four explicit water molecules, and the substrate. Via computations, the persistence of the short-lived five-coordinate phosphorane intermediate on the minutes times scale is rationalized. This five-coordinate phosphohistidine intermediate energetically exists between the hydrolysis event and ″substrate reorganization″ (the reorganization of the *in vitro* model substrate within the active site). Computations directly support the thermodynamic favorability of the *in vitro* four-coordinate phosphohistidine product. *In vivo*, the activation energy of substrate reorganization is too high, perhaps due to a combination of substrate immobility when embedded in the lipid bilayer, as well as its larger steric bulk compared to the compound used in the *in vitro* substrate soaks. On this longer time scale, the enzyme will migrate along the lipid membrane toward its next substrate target, rather than promote the formation of the dead-end product.

INTRODUCTION

The HKD Phospholipase D superfamily is one of four members of the phospholipase enzyme class and is known to cleave the headgroup of phosphatidylcholine (PC) to produce phosphatidic acid (PA) and choline. This cleavage is known as Phospholipase D (PLD) hydrolysis. Via this molecular transformation, PLD is a crucial enzyme in numerous biochemical pathways involving cell signal transduction, mitosis, metabolism, and secretion.[1] Enzymes with PLD activity can also be used to catalyze transphosphatidylation of PC on an industrial scale.[2,3] The over 4000 currently sequenced proteins belonging to the PLD superfamily within the GenBank (NCBI) database[4] is confirmation that PLD is ubiquitous in most forms of animal, plant, and bacterial life. Yet a coherent story regarding the biochemical function of the PLD superfamily, as well as the pharmaceutical and industrial potential of enzymes with Phospholipase D activity, is only recently taking shape, exemplified by comprehensive reviews published since 2002.[1,3,5] Furthermore, a detailed chemical understanding of the catalytic mechanism and function of HKD PLD on the atomic scale is still incomplete.

The first identification of PLD activity in plants was reported in 1947 by Hanahan and Chaikoff,[6] while the first identification in an animal was reported by Saito and Kanfer in 1975.[7] Isolation of human PLD occurred shortly thereafter via the work of Kater et al.[8] Consensus about possible mechanistic pathways converged with the discovery of a highly conserved ″$HxKxxxxDx_6GSxN$″ set of residues (the ″HKD″ sequence motif) near the active site.[9,10] The HKD motif often occurs

Received: April 29, 2013
Published: September 5, 2013

dx.doi.org/10.1021/ja4042753 | J. Am. Chem. Soc. 2013, 135, 13764−13774

once in lower-order enzymes that form homodimers when catalytically active (e.g., Nuc)[11] and twice within the sequence of higher order PLD enzymes (e.g., mammalian PLD).[10] In fact, authors of a recent PLD review propose that the existence of one or two HKD-like sequences in a phosphodiesterase is the primary criterion for inclusion in the PLD superfamily: "[h]istorically, many bacterial virulence factors that demonstrated the release of a choline headgroup were named PLDs for this function." Enzymes that lack the HKD sequence motif are not members of the PLD superfamily.[1]

Dixon, Gottlin, and coauthors[12] provided a convincing argument for a phosphohistidine intermediate, versus a free sulfhydryl phosphatidate acceptor proposed in early literature.[13] Their results also suggested that the intermediate was five-coordinate. The concept of a phosphohistidine intermediate gathered further support upon the published crystallization of Nuc.[11] Next, a major breakthrough in the structure and mechanism of the PLD superfamily occurred when Leiros, McSweeney, and Hough, building upon preliminary work,[14,15] crystallized (at resolutions of 1.35−1.75 Å) a series of structures from *Streptomyces sp.* PMF (PLD_{PMF}) along the reaction pathway.[16] The main residues involved in the catalysis were unequivocally identified in PLD_{PMF}, and presumably the entire PLD superfamily. These residues are, according to the sequence numbering, of PLD_{PMF}, H170, K172, D473, N187, H448, K450, D202, and N465. This set of eight residues forms a nearly C_2 symmetric "cage" around the phosphodiester substrate (Scheme 1). The native species, along with a series of inhibited, substrate-soaked, and product-soaked X-ray crystal structures (8 total) were elucidated and refined.

Scheme 1

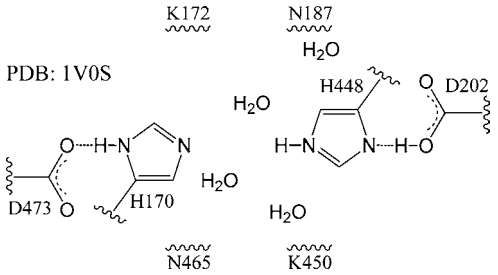

Enzyme-catalyzed phosphoryl transfer mechanisms, which have been a subject of intense debate for decades,[17,18] can be divided into three extremes, (1) fully dissociative (or S_N1-type) mechanisms, where a three-coordinate metaphosphate intermediate is formed, (2) fully associative (or S_N2-type) mechanisms, where a five-coordinate phosphorane intermediate is formed, and (3) concerted mechanisms without intermediates. From substrate soaking experiments, an X-ray crystal structure of a five-coordinate intermediate was isolated and characterized by Leiros et al.[16] This species indicates an associative mechanism for PLD_{PMF} and presumably most, if not all, members of the PLD superfamily.

Surprisingly, Leiros et al. isolated a "dead-end" four-coordinate phosphohistidine product that forms between one-half hour of substrate soak and eight hours of substrate soak. They concluded that the H170 residue was nucleophilic enough to reform the covalent $P-N_{H170}$ bond between the hydrolyzed substrate mimic (dibutyrylphosphatidic acid, diC_4PA) and perform a second phosphoryl transfer reaction. This second phosphoryl transfer cleaves the entire diacylglycerol moiety, suggesting that PLD_{PMF} effectively functions as a phospholipase C/phosphodiesterase within the *in vitro* crystallization conditions. Leiros et al. hypothesized that substrate reorientation/reorganization or "substrate aging" could promote this second phosphoryl transfer.[16] Based on the observed phosphohistidine intermediate, the basic chemistry of the proposed mechanism is believed to proceed through a series of associative intermediates.[16,19] A schematic of the overall mechanism is shown in Figure 1 where the *in vivo* mechanism is colored in black and the additional *in vitro* termination of catalysis is colored in red. Figure 1 provides an overview of the gross mechanistic steps that are the basis for our theoretical work.

In the current article, we have developed a nineteen amino acid residue quantum mechanical cluster model[18,20] of the PLD_{PMF} enzyme utilizing the ONIOM QM:QM methodology. These computational models are employed to elucidate the activation free energies and typical reaction profile of phospholipid hydrolysis by enzymes of the PLD superfamily. This model encompasses the relevant PLD_{PMF} residues (including the two active-site HKD-motifs, explicit water molecules, and substrate) that are directly involved in the hydrolysis reaction through covalent or hydrogen bonding.

COMPUTATIONAL METHODS AND MODEL BUILDING

All computations were performed using the Gaussian09[21] software packages. In ONIOM optimizations,[22] the "high-level" layer was allowed to freely optimize using Density Functional Theory (DFT) with the hybrid B3LYP functional.[23] The 6-31G(d') basis set was used for N, O, and P atoms,[24,25] while 6-31G was used for C and H atoms. Atoms in the "low-level" layer atoms were constrained in their crystallographically determined positions and treated with the PM6 semiempirical Hamiltonian.[26]

The structural basis of our computations was to begin with the PLD_{PMF} X-ray crystal structure obtained via the 30 min soak of diC_4PC substrate (PDB code = 1V0Y).[16] To create an appropriate high-level layer, it was necessary to include two explicit solvent molecules that directly hydrogen bond to the reaction site, (1) the water molecule interacting with both N187 and H448 (referred to by its PDB name wat2207), and (2) the water molecule interacting with H448, N465, and K450 (wat2413). Leiros et al.[16] also commented that the C-terminus serine (S463) belongs to the important GG/GS motif.[27] The S463 residue does not directly participate in the catalysis, but holds H170 in the proper orientation for nucleophilic attack of the phospholipid substrate. Our preliminary results indicated that inclusion of S463 in the model was necessary for stabilization of the hydrogen bonding between D473 and H170. This stabilization facilitates $P-N_{H170}$ bond dissociation/formation and subsequent removal of the phosphoryl group.

Carrea et al. purified PLD_{PMF} and examined the effect of pH on relative activity.[28] PLD_{PMF} was shown to be most active between the pH range of 4−6, where the substrate would exist in its dihydrogen phosphate ion form ($H_2PO_4^-/R_2PO_4^-$), and accordingly the crystallization experiments were performed near a pH of 5.4.[14,16] With a proton able to transfer between H170/D473 and H448/D202, and the two lysine residues protonated, the empty active site has an overall +1 charge. When the monoanionic substrate $[P(O)_2(OR^1)(OR^2)]^-$ is included, the overall computational model with substrate and enzyme becomes neutral. In the article, "OR^1" will designate the substrate ligand involved in the first phosphoryl transfer, and "OR^2" will designate the ligand involved in the second phosphoryl transfer. The choline headgroup and dibutyryl-containing triglycerol R-groups of the *in vitro* substrate, diC_4PC, are trimmed to methoxy ligands. Therefore, $OR^1 = OR^2 = OCH_3$. Overall, the high-level layer (with substrate) contains less than 100 atoms: 98 atoms with $[P(O)_2(OCH_3)(OCH_3)]^-$, henceforth $P(O)_2(OR^1)(OR^2)$; and 95 atoms with a $[P(O)_2(OCH_3)(OH)]^-$, henceforth $P(O)_2(OR^2)(OH)$.

dx.doi.org/10.1021/ja4042753 | J. Am. Chem. Soc. 2013, 135, 13764−13774

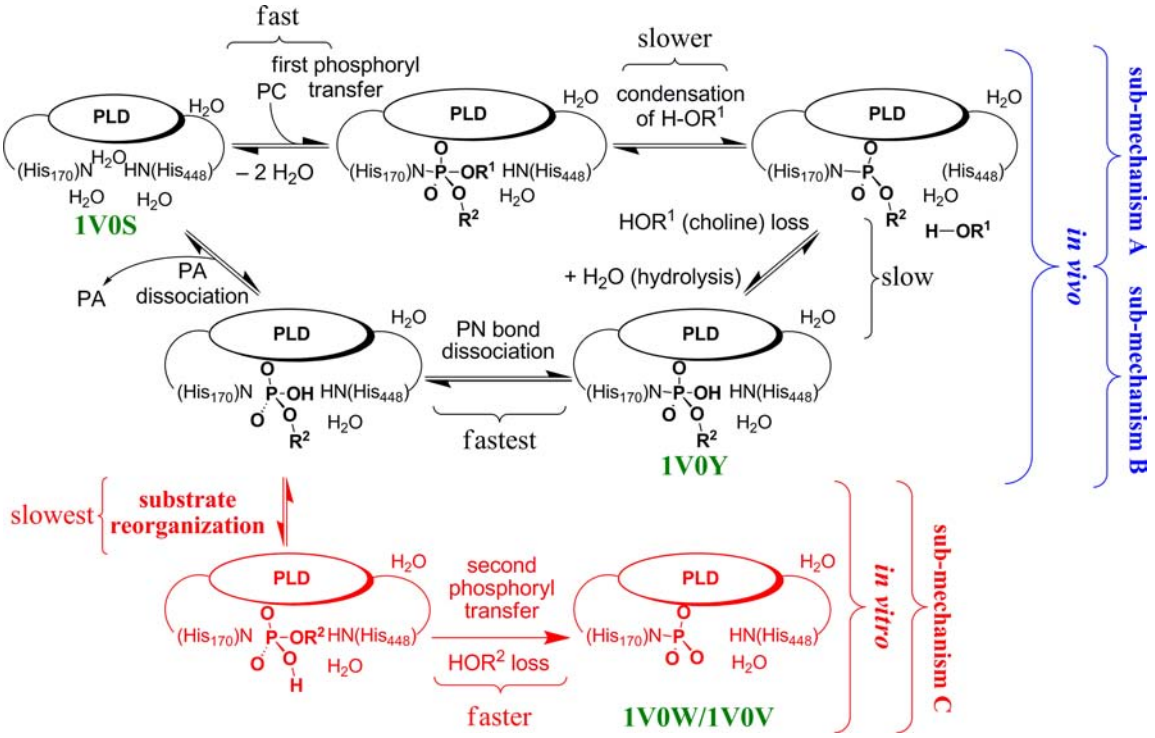

Figure 1. "Cloud" model schematic of the overall investigated *in vivo/in vitro/in silico* chemical processes that apply to the PLD superfamily of enzymes for the hydrolysis of phosphatidyl choline (PC). When R^1 is cholinate and R^2 is diacylglycerol backbone, PLD hydrolysis of PC substrate yields phosphatidic acid (PA) and choline. Green label identifies the species observed in the X-ray crystal structure. **Submechanism A** and **submechanism B** correspond to the *in vivo* part of the mechanism, while **submechanism C** corresponds to the *in vitro* part of the mechanism (see Figure 5). Not pictured: if water in the *in vivo* hydrolysis step is replaced with primary alcohol, PLD transphosphatidylation of PC yields a phosphatidylalcohol.

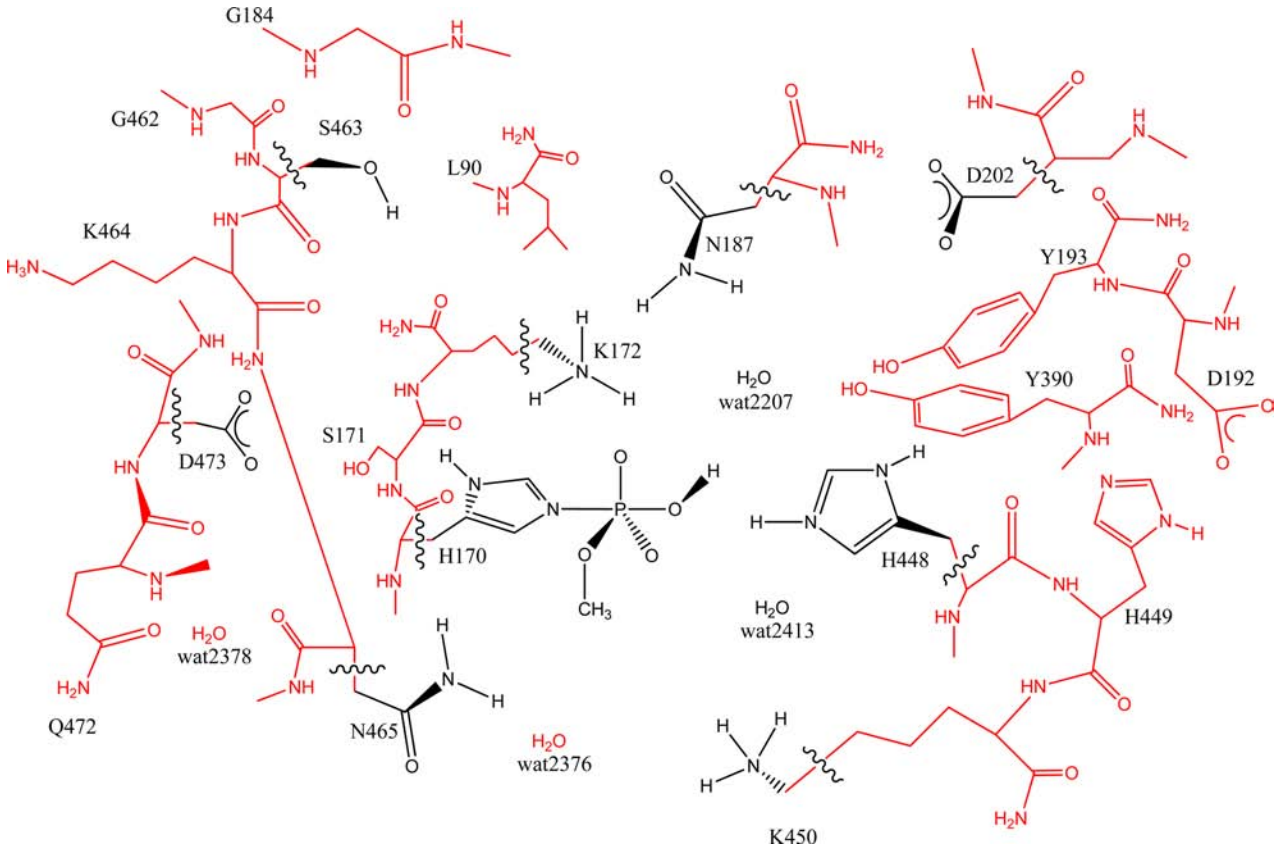

Figure 2. 2D model representation of the optimized structure **B-2**.

dx.doi.org/10.1021/ja4042753 | J. Am. Chem. Soc. 2013, 135, 13764–13774

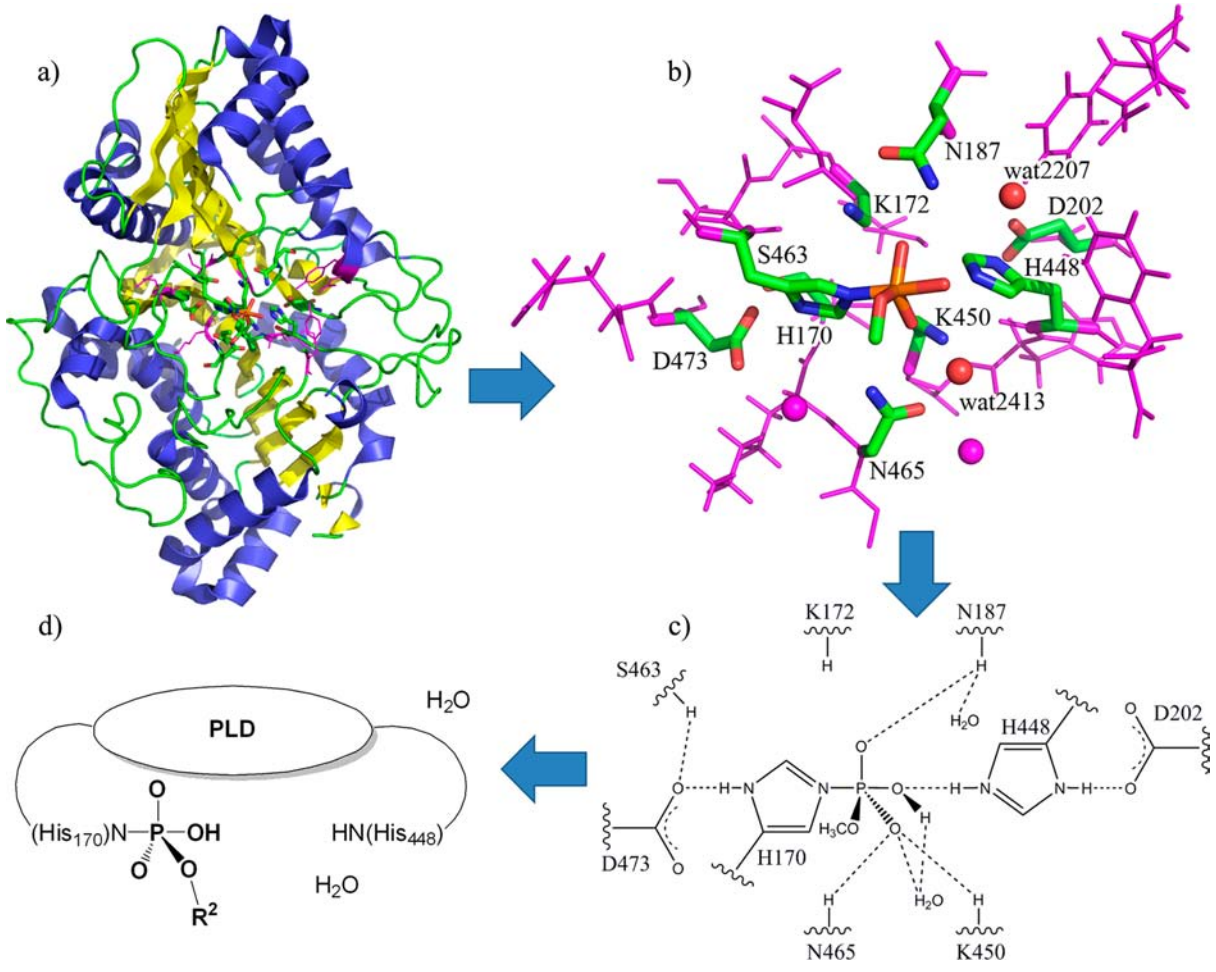

Figure 3. Various 2D/3D representations of phospholipase D. (a) The tertiary structure of 1V0Y, (b) trimmed 3D model with ″low-layer″ atoms in magenta, (c) ″block″ 2D model, and (d) ″cloud″ 2D model.

The low-level layer, which consisted of the remaining atoms, contains ten additional amino acid residues (L90, S171, G184, D192, Y193, Y390, H449, G462, K464, and Q472) and two additional explicit solvent water molecules (labeled wat2376 and wat2378 in the PDB file). Peripheral atoms on some distant residues were truncated to reduce the size of the models and maintain neutral charge, and altogether the low-level layer contained 305 atoms. This model retains the electronic and steric characteristics of the active site ″pocket″ without necessitating extreme amounts of conformational complexity in the phosphoryl ″R″ groups. The solvent water molecules labeled wat2207 and wat2413, and the entire *in silico* substrate are unconstrained in all geometry optimizations. A 2D picture of the full ONIOM QM:QM model is shown in Figure 2, which can be compared to the 3D model (and simplified 2D representations) in Figure 3.

All models were geometry optimized in the gas phase using standard gradient methods. The energy Hessian was evaluated at all stationary points to designate them as either minima or transition states at the computed level of theory. But for a few exceptions (*vida infra*), reported minima all have real frequencies, and transition states have one imaginary frequency. Reported zero-point corrected energies and free energies are reported at 298.15 K and 1 atm and were determined using the computed, unscaled harmonic vibrational frequencies. Protein solvation energies were computed using the COSMO polarizable conductor model (PCM)[29] with UAKS sets of atomic radii,[29] a nondefault electrostatic scaling factor of 1.2, and a dielectric constant of $\varepsilon = 4.0$ to simulate the less-polarized protein environment.[30] Fully quantum mechanical B3LYP gas-phase and PCM single-point computations on ONIOM B3LYP:PM6 geometry-optimized stationary points were used to obtain solvation free energies for all species. These fully QM computed solvation free energies were combined with the free energies derived from ONIOM B3LYP:PM6 geometry optimizations to obtain free energies of solution, $\Delta G^{\circ/\ddagger}_{(\mathrm{QM//ONIOM\ QM:QM\ soln})}$ (see SI for further details).[31] Initially, we performed an exhaustive, manual, and fully quantum-mechanical conformational search of a trimmed model equivalent to the high-layer PLD model. These structures were used as starting guesses for the high-layer of the ONIOM QM:QM optimizations. All values reported in the text are $\Delta G^{\circ/\ddagger}_{(\mathrm{QM//ONIOM\ QM:QM\ soln})}$. A native enzyme active site model with close geometric and hydrogen-bonding network similarity to 1V0S and 1V0Y X-ray crystal structures was used for the thermodynamic comparison.

Hatanaka et al. have previously stated that enzymes in the PLD superfamily may undergo significant conformational change before and after phosphoryl transfer.[32] However, there is little conformational change in the pertinent active site residues when overlaying the native enzyme 1V0S with 1V0Y. The most significant structural shift between the two is the location of several solvent water molecules that occupy the region of the substrate oxygen atom positions of 1V0Y. The RMS deviation of the nine constrained atoms in our trimmed 1V0Y model versus the same crystallographic locations of these atoms in 1V0S (native enzyme X-ray crystal structure)[16] is only 0.201 Å. In fact, except for the disordered H170 in 1V0W, the active sites of 1V0S, 1V0Y, 1V0W, 1V0V, 1V0T, and 1V0U X-ray crystal structures all show qualitatively similar structural overlays. This similarity suggests only minor conformational changes of the enzyme in the local region of the active site, once $\mathrm{PLD}_{\mathrm{PMF}}$ is in the proper activated form for substrate recognition. Therefore, the 1V0S-like native enzyme computational

dx.doi.org/10.1021/ja4042753 | J. Am. Chem. Soc. 2013, 135, 13764−13774

model will also have truncated residues with frozen carbon at the 1V0Y crystallographic position in order to appropriately compare relative energies. Finally, in order to balance reaction energies between the complete catalytic cycle of phosphoryl transfer and hydrolysis, PLD models of the native enzyme active site were constructed with two extra explicit water molecules (six waters total).

RESULTS AND DISCUSSION

Preface A – Visualization of Results. The accurate two-dimensional depiction of an enzyme active site is fraught with difficulties in terms of convention and perspective. Clearly, both the 2D and 3D models depicted in Figures 2 and 3 show a crowded active site. From our experience over the course of enzyme mechanism investigations, utilization of these large cartoons can easily obfuscate the description of the reaction mechanism, even without the low-layer (and background protein turns and helixes). Instead, throughout the main text a simplified ″cloud″ model is used for our schemes, where only the substrate bond breaking/forming processes from the geometry optimizations are explicitly shown. 2D diagrams constructed with a ″block″ model depicting the minimal hydrogen bonding of the active site residues, substrate, and water molecules are included in the Supporting Information (Figures S1–S3). Figure 3 contains various useful representations of 1V0Y, including the representation of the tertiary structure of the X-ray crystal structure, the trimmed 3D model, the ″block″ 2D model, and the ″cloud″ 2D model.

Preface B – Chemical Context of the Proposed Mechanism. The overall mechanism can be more easily described when broken down into three ″submechanisms″. A thorough description of thermodynamics, kinetics, and solution phase energies of the submechanisms will be discussed separately in the Results and Discussion sections *b* through *d*. The first two submechanisms will correspond to the *in vivo* catalytic cycle for the hydrolysis of PC to yield PA and choline (Figure 1): the substrate–enzyme bonding and first phosphoryl transfer in Section b, and the hydrolysis event in Section c. In Section d, the second phosphoryl transfer, occurring only *in vitro* (Figure 1 – red), will be discussed. These three submechanisms are separated by processes for which direct transition states will not be located computationally. Specifically, between the first phosphoryl transfer and hydrolysis, the cleaved headgroup (HOR^1, where $R^1 = CH_3$ *in silico* and R^1 = choline *in vivo/in vitro*) will exit the active site and be replaced by an incoming water molecule. In the hydrolysis and second phosphoryl transfer mechanisms, R^1 = H. Between the hydrolysis event and the second phosphoryl transfer, the equatorial OH and the axial OR^2 of the *unbound* substrate switch positions, that is the substrate must be ″reorganized″.

In the PLD_{PMF} crystallization experiments, the catalysis environment contained the buffer-soluble diC_4PC substrate in concentrations many orders of magnitude higher than the enzyme. On the other hand, *in vivo*, solitary monomers of aqueous phase substrate (as well as the enzyme itself) would exist in concentrations many orders of magnitude less than substrate found embedded into the lipid bilayer.[14–16,33] As noted by Selvy et al., if bulk lipid concentration is considerably larger than the interfacial binding, then Michaelis–Menten kinetic assumptions can be valid.[1] In contrast to *in vitro* experiments where Michaelis–Menten kinetics applies, the *in vivo* catalytic cycle is a more complicated process involving interfacial kinetics, or ″scooting″ along the lipid bilayer, as well as subsequent enzyme activation from a lipid binding cofactor.[1,33,34] The substrate presentation kinetics of phospholipases is an ongoing and active area of research.[33–35] Mechanisms in the current article are postulated in the context of the *in vitro* catalytic cycle. Thus, our discussion centers on the thermochemistry and kinetics of phosphoryl transfer and hydrolysis independent of substrate presentation and enzyme–bilayer interactions.

(a). Beginning of the Catalytic Cycle of PLD_{PMF}. In order to properly model a conserved thermodynamic cycle for the three submechanisms, it is first necessary to model the native enzyme active site (i.e., without substrate). This empty active site will provide a reference energy for the catalytic cycle and will be useful for determining the substrate binding energy. Substrate migration into the active site and displacement of water is an entropically favored process. Overlays of the 1V0S and 1V0Y X-ray crystal structures show three water molecules in 1V0S that are positioned very near the locations of the equatorial oxygen atoms of the five-coordinate phosphohistidine intermediate (1V0Y), with an RMSD of 0.60 Å from the positions of the three equatorial phosphoryl oxygen atoms. In our computational model, two of these waters will be ″pushed out″ of the active site by incoming substrate, and the third explicit water molecule will become wat2413. Therefore, our overall reaction scheme is balanced by the loss of two water molecules when placing substrate in the model of 1V0S (Figure 1).

(b). Formation of Phosphohistidine Intermediate. Our discussion will focus on the most structurally viable and energetically preferred pathway (submechanism A) based on the orientation of H170 and the position of wat2207 compared to their positions in 1V0Y. The X-ray crystallographic study performed by Leiros et al. suggests a set of *in vivo/in vitro* associative phosphoryl transfers due to the structure of the 1V0Y intermediate analogue. Indeed, our exploration of the PLD_{PMF} conformational space explicitly rules out dissociative mechanisms because no three-coordinate metaphosphate intermediates were *ever* located. Likewise, no direct interchange five-coordinate phosphorane transition states were *ever* located.[36]

At the beginning of the catalytic mechanism, the model $P(O)_2(OR^1)(OR^2)$ substrate enters the active site and becomes part of the ″supermolecule″ (**A-1**). We have made no attempt to model the diffusion mechanism and kinetics, and we begin discussing the reaction mechanism with an uncomplexed $P(O)_2(OR^1)(OR^2)$ substrate. Detailed 2D ″block″ diagrams corresponding to changes in hydrogen and covalent bonding of the directly participating residues are given for all submechanisms in Supporting Information, and submechanism A is described in Figure S1. The **A-1** structure leads to the transition state of PN bond formation (**A-TS-1-2**) via attack of the substrate phosphorus atom by the *tele* N atom of H170 (Scheme 2).[37] This transition state has a solution-phase activation free energy of 15.1 kcal mol^{-1} compared to the

Scheme 2

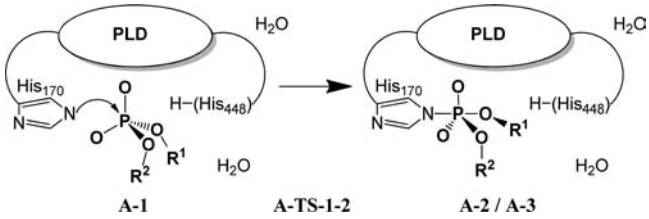

dx.doi.org/10.1021/ja4042753 | J. Am. Chem. Soc. 2013, 135, 13764–13774

initial supermolecule **A-1**. Interestingly, the first five-coordinate structure (**A-2**) is a transient intermediate[38] that is essentially isoenergetic with **A-TS-1-2** and possesses a long PN bond distance of 2.13 Å. Via a presumably low-energy rotation of the OR^1 methoxy ligand and approach of the substrate to a PN distance of 2.01 Å, the (**A-3**) structure is formed, which is 16.2 kcal mol^{-1} higher in free energy than **A-1**.

The phosphohistidine intermediate is next activated by the proton on H448 (**A-TS-3-4**) and general-acid catalysis occurs (Scheme 3) with a $\Delta\Delta G$ of 4.1 kcal mol^{-1} compared to **A-3**.

Scheme 3

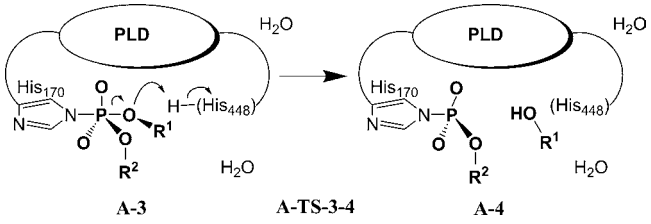

Phosphoryl transfer is completed during the condensation when the OR^1 ligand is cleaved from the intermediate and the newly four-coordinate intermediate (**A-4**) takes on a pseudotetrahedral arrangement. The "product" of this submechanism is significantly higher in free energy than **A-1**, $\Delta\Delta G$ = 13.0 kcal mol^{-1}. The first submechanism ends here with four-coordinate phosphorus, Enzyme-$N_{H170}P(O)_2(OR^2)$, and a free HOR^1 molecule (choline).

(c). Hydrolysis. At this point in the reaction, the free HOR^1 (choline *in vivo* and *in vitro*, methanol *in silico*) migrates out of the active site and is replaced by a water molecule from the bulk solvent. This new water molecule is hydrolyzed during the attack on the phosphorus of the four-coordinate phosphohistidine intermediate to form a new five-coordinate Enzyme-$N_{H170}P(O)_2(OR^2)(OH)$ intermediate (Scheme 4). All computed hydrolysis transition states and five-coordinate intermediates are consistent with a fully associative mechanism. In this section, the most energetically favorable pathway of submechanism B will be discussed in detail and all 2D structures are presented in Figure S2.

Scheme 4

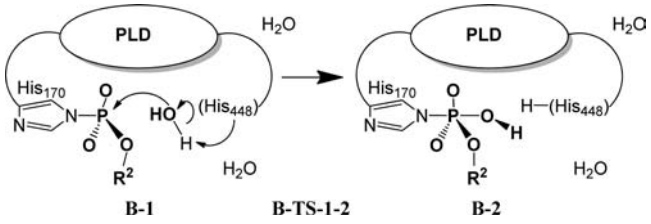

The first structure has a bound tetrahedral four-coordinate $P(O)_2(OR^2)(OH)$ intermediate (**B-1**). When balancing the catalysis stoichiometrically (via loss of OR^1 and addition of H_2O to form **B-1**), the relative free energies of **B-1** ($\Delta\Delta G$ = 14.6 kcal mol^{-1} compared to **A-1**) and **A-4** ($\Delta\Delta G$ = 13.0 kcal mol^{-1}) are quite similar. The incoming water molecule is activated by H448, and undergoes a concerted reaction where OH is added to the phosphorus and the nucleophilic nitrogen atom on the H448 imidazole ring abstracts a proton (**B-TS-1-2**). The fairly long bond distances, $r_e(P{-}O_{axial})$ = 2.778 Å and $r_e(N_{H448}{-}H)$ = 1.784 Å, suggest a rather early transition state. For this hydrolysis TS, the relative free energy of activation is $\Delta\Delta G$ = 18.1 kcal mol^{-1}.

This five-coordinate phosphohistidine intermediate (**B-2**) has an apical OH group and an equatorial OR^2 group. This five-coordinate intermediate very closely resembles the 1V0Y X-ray crystal structure. Including all unconstrained heavy atoms in the high layer, the RMSD of **B-2** compared to 1V0Y is only 0.42 Å. When the two water molecule oxygen atoms and the carbon atom of OR^2 are excluded, the RMSD of the remaining 30 atoms is only 0.21 Å (see Figure 4 for the overlay). **B-2** is

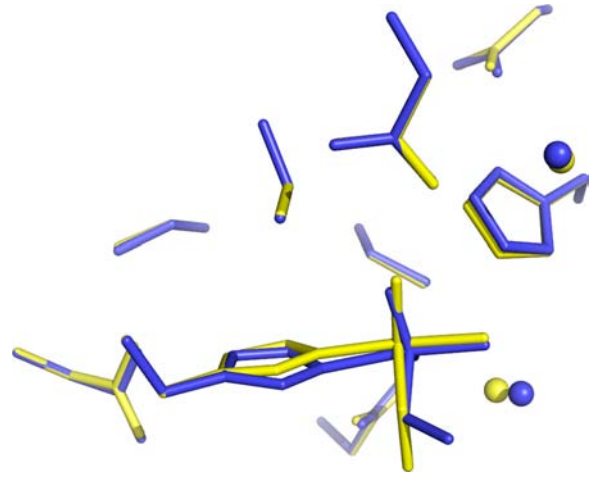

Figure 4. Overlay of 1V0Y X-ray crystal structure (yellow) and **B-2** (blue). For clarity, hydrogen atoms are removed and only unconstrained "high-layer" atoms are shown.

effectively identical to the geometry observed in the 1V0Y X-ray crystal structure (there is a small difference for wat2413 and a slight rotation of the equatorial OR^2 group).

In the experiments carried out by Leiros et al., the triglycerol group of the hydrolyzed diC_4PC phospholipid (converted to a diC_4PA-containing structure) is similarly equatorial in the 1V0Y crystal structure (the freed choline headgroup has already departed the active site). At this point *in silico*, the transition state of $P{-}N_{H170}$ bond dissociation (**B-TS-2-3**) is very early and facile, $\Delta\Delta G$ = 0.6 kcal mol^{-1} (Scheme 5). The overall

Scheme 5

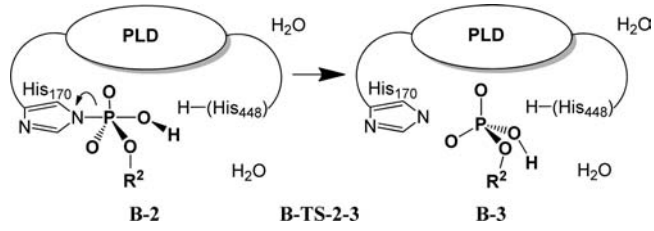

reaction is exergonic (ΔG = −5.5 kcal mol^{-1}) when comparing the final intermediate (**B-3**) to the initial supermolecule "reactant" (**A-1**). In the biological catalytic cycle, the enzyme, controlled by the interfacial kinetics, migrates to its next PC target along the lipid bilayer.

(d). Dead-End Product. Upon *in vivo* hydrolysis and release of PA, the biological catalysis would be completed (Scheme 6).[1,39] However, in the experiments of Leiros et al., at a time between 30 min and 8 h of soaking PLD_{PMF} with diC_4PC, an unexpected product forms.[16] The X-ray crystal structures

dx.doi.org/10.1021/ja4042753 | J. Am. Chem. Soc. 2013, 135, 13764−13774

Scheme 6

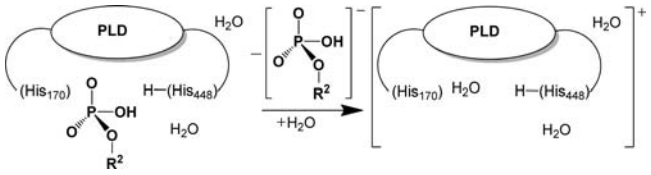

isolated and characterized from 8-h and 8-day substrate soaks (1V0W and 1V0V, respectively) are extremely similar to the X-ray crystal structures isolated using a glycerophosphate product soak (30 min for 1V0T; 90 min for 1V0U). In the latter two X-ray crystal structures, a phosphoryl group is observed to be covalently bound to H170, suggesting reorientation of the $P(O)_2(OR^2)(OH)$ glycero substrate (through substrate reorganization, Scheme 7), formation of the $P-N_{H170}$ bond

Scheme 7

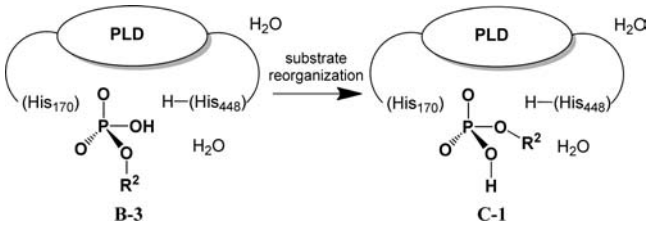

Scheme 8

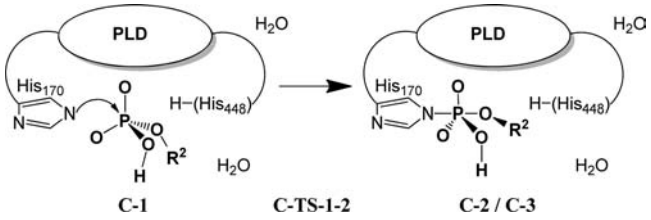

Scheme 9

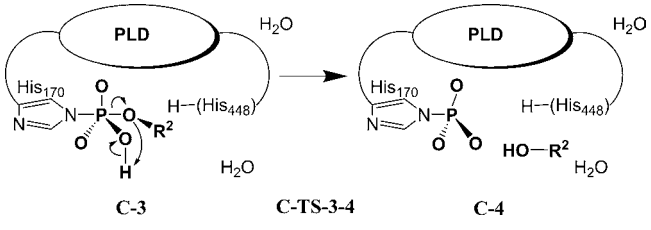

(Scheme 8), and cleavage of OR^2 (Scheme 9). This submechanism proceeds stoichiometrically, and the final $P(O)_3$ phosphohistidine dead-end product is formed.

In this section, the proposed mechanism for submechanism C will be discussed in detail and all 2D structures are shown in Figure S3. Substrate reentry affords **C-1**, with the substrate reoriented with an equatorially disposed hydroxyl ligand and poised for nucleophilic attack of the phosphorus by the *tele* N_{H170}. The free energy of activation for the $P-N_{H170}$ bond formation (see **C-TS-1-2** in Scheme 8) is 16.0 kcal mol^{-1}. Once the five-coordinate intermediate (**C-2**) is formed, a minor conformational change of the N465 residue and wat2413 occurs to produce **C-3** (via **C-TS-2-3**, not shown; see Figure S3). The subsequent transition state of the second phosphoryl transfer in Scheme 9 (**C-TS-3-4**) has interesting features. The participating proton on H448 is not acidic enough to activate the intermediate. Due to the relatively low activation free energy necessary to break the $P-N_{H170}$ bond ($\Delta\Delta G$ = 4.3 kcal mol^{-1}), the leaving OR^2 group instead removes the proton from the equatorial OH ligand. Thus, the H170-bound four-coordinate phosphohistidine lacks any protons (**C-4**), while free alcohol (HOR^2) is released from the active site. From this final dead-end product comes a stabilization of −9.8 kcal mol^{-1} in free energy compared to **A-1**.

(e). Full Reaction Kinetics and Thermodynamics. Now that the chemical transformations of the submechanisms have been described, the thermodynamics and kinetics of the overall catalytic process will be discussed. It is first of interest to compare the quantum mechanical (ONIOM QM:QM) cluster model substrate binding energies with a molecular mechanical docking study carried out by Reilly and coauthors.[40] In that paper, computations were performed with the PO_4-inhibited PLD_{PMF} crystal structure (1F0I) and Amber_95 partial charges. Various phospholipids known to be hydrolyzed by PLD were docked to the enzyme in order to assess relative binding energies. With five different headgroup types, Reilly found a monotonic increase in the magnitude of the binding energy with increasing fatty acid chain length. Their docking simulations of phospholipids with various head groups and fatty acid chains truncated to methoxy ligands gave a range of binding energies from −35.4 to −122.7 kcal mol^{-1}. This gives a reasonable range of binding energies to compare to our ONIOM QM:QM cluster model.

In the catalytic mechanism, the reference energy is the enzyme/unbound substrate supermolecule with two infinitely displaced solvent water molecules (**A-1**). Compared to the appropriate reference native enzyme structure (Scheme 1) plus infinitely separated substrate, the gas phase free energy of substrate "diffusion" (Scheme 10) is computed to be −63.1

Scheme 10

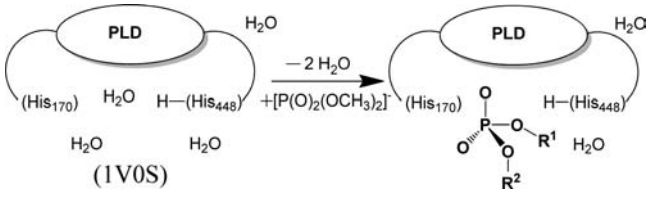

kcal mol^{-1}.[40] Charge separation effects of the anionic substrate and cationic native active site model will be exacerbated in the gas phase. Thus, the free energy of bringing the substrate into the active site is computed to be free energy favored, but less so (−16.7 kcal mol^{-1}) in solution. This solution phase binding energy (from our trimmed *in silico* model substrate) is qualitatively acceptable, near the higher (less negative) values of smaller substrates in the investigation of Reilly and coauthors.[40]

In Figure 5, stoichiometrically appropriate relative free energies of the total reaction mechanism (**submechanisms A**, **B**, and **C**) are shown for the solution phase computations. Three possible hypotheses are available to rationalize the existence of the 1V0Y and 1V0W crystal structures. The first hypothesis is that the substrate reorganizes directly from **B-2** to **C-2**; the second hypothesis is that five-coordinate intermediate resides in a stable free energy basin; and the third hypothesis is that the *in vitro* hydrolyzed model substrate (diC_4PA) is slow to migrate from the active site.

dx.doi.org/10.1021/ja4042753 | J. Am. Chem. Soc. 2013, 135, 13764−13774

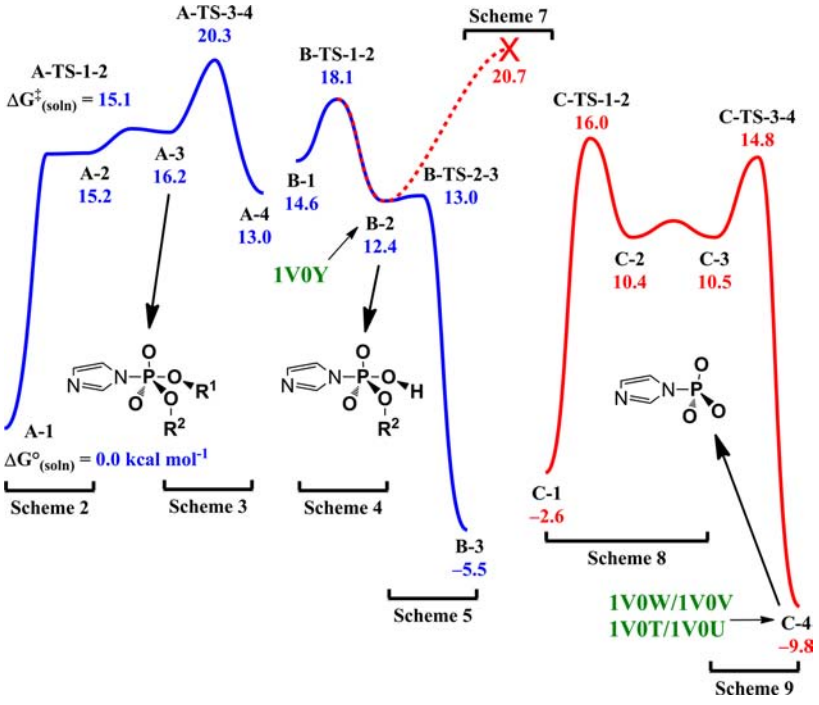

Figure 5. Free energy diagram for the proposed mechanism for PLD_{PMF}. $\Delta G^{\circ/\ddagger}_{(soln)}$ corresponds to the $\Delta G^{\circ/\ddagger}_{(QM//ONIOM\ QM:QM\ soln)}$ given in the text. The persistence of the 1V0Y X-ray crystal structure on the time scale of minutes is rationalized by the free energy basin (in dotted red) between **B-TS-1-2** and "substrate reorganization" (i.e., conversion of **B-3** to **C-1**). The red "X" marks the location of the approximate $\Delta G^{\ddagger}_{(soln)}$ of substrate reorganization. Blue and red solid lines signify the relationship between *in vivo*, *in vitro*, and *in silico* proposed mechanisms. Green labels (PDB codes) below the species identify a resemblance to the computed geometry and those observed in the X-ray crystal structure (see Figure 1). Note that geometry optimized **C-4** contains HOR^2, whereas the leaving alcohol is not present in 1V0W/1V0V/1V0T/1V0U.

The first hypothesis is that the substrate reorganizes directly from **B-2** to **C-2**. The five-coordinate phosphohistidine intermediate (**B-2**) could undergo a series of turnstile rotations (which would result in a stereomutation). However, the active site lysine and arginine residues sterically eliminate most possibilities for square−pyramial transition states that would interchange the OR^2 ligand from the apical to the equatorial position. We considered the detailed conformational flexibility of the active site and its effects on the phosphoryl transfer mechanisms by modeling the "high-level" layer only. A few sterically allowed square-pyramial transition states were located, but were 22−29 kcal mol^{-1} higher in free energy than the respective **C-TS-1-2**-like transition states. Also, the resulting minima had oxo ligands switched with OH/OR, so that OH/OR ligands were no longer oriented properly to be activated by H448 (Figure S4a). Furthermore, no direct transition states were found for equatorial-to-apical OH/OR^2, O/OR^2, or OR^1/OR^2 stereomutation (Figure S4b). Therefore, the possibility of reorganization of the five-coordinate phosphohistidine intermediate is implausible.

The second hypothesis is that after the hydrolysis of the four-coordinate $P(O)_2(OR^2)$ intermediate (formation of **B-2**), the resultant five-coordinate Enzyme-$N_{H170}P(O)_2(OR^2)(OH)$ intermediate would reside in a stable free energy basin. For this hypothesis to be validated computationally, the transition states of hydrolysis and $P-N_{H170}$ bond dissociation would both have the two highest free energies of activation of the total reaction mechanism. According to our ONIOM QM:QM computations, this is not the case. The activation free energy ($\Delta\Delta G$ = 0.8) of the $P-N_{H170}$ bond dissociation of the hydrolyzed product (**B-TS-2-3**) is surprisingly negligible.

While our computations agree with crucial mechanistic interpretations of the 1V0Y X-ray crystal structure data,[16] the hydrolysis of the four-coordinate phosphohistidine intermediate is not the catalytic rate-determining step as has been suggested in the literature, but rather the *first phosphoryl transfer* (**A-TS-3-4**, $\Delta G^{\ddagger}_{(soln)}$ = 20.3 kcal mol^{-1}). The hydrolysis transition state has the second largest free energy of activation (**B-TS-1-2** $\Delta G^{\ddagger}_{(soln)}$ = 18.1 kcal mol^{-1}). This result suggests that a low energy basin should exist between the first phosphoryl transfer and the hydrolysis, and an intermediate analog crystal structure should resemble the pseudotetrahedral four-coordinate intermediates, while OR^1 is exchanging with the bulk solvent (**A-4** and **B-1**). We have also obtained low-energy structures connected to **B-3**, where the H170 residue mimics the conformational change that occurs when PLD becomes inhibited by phosphate *in vitro* (akin to the 1F0I X-ray crystal structure).

The third hypothesis is that the *in vitro* hydrolyzed model substrate (diC_4PA) is slow to migrate from the active site. However, this migration is slow enough to allow for the observation of the five-coordinate intermediate *and* fast enough to allow for substrate reorganization. In the crystallization experiment, high concentrations of model substrate were used (~2−3 mM of diC_4PC and 0.1 M of phosphate inhibitor). Our results suggest that "substrate reorganization" becomes the *rate-limiting, yet surmountable kinetic step* of the stoichiometric formation of dead-end product (Figures 1 and 5). The activation free energy of substrate reorganization is approximated as the free energy change of removing $PO_2(OR^2)(OH)$ from the active site [from **B-3** to infinitely separated 1V0S and $PO_2(OR^2)(OH)$], which is computed to be 20.7 kcal mol^{-1}. This free energy of "dissociation" approximates the free energy

dx.doi.org/10.1021/ja4042753 | J. Am. Chem. Soc. 2013, 135, 13764−13774

required for this rate-limiting step of substrate reorganization. Explicitly determining the free energy of activation for the diffusional process is complicated by a gradient in substrate-solvent interactions from the protein environment to the bulk solvent, as well as possible limitations in our computational model. Thus, this value of 20.7 kcal mol^{-1} also approximates an upper limit of free energy of activation for the diffusional process.

Overall, the transformation of PC [the $P(O)_2(OR)_2$ substrate] and subsequent water addition/hydrolysis are kinetically fast (1V0S to 1V0Y). *In vivo*, PLD catalyzes the choline headgroup hydrolysis and removal of PA occurs with high specificity (back to native enzyme 1V0S). The selectivity of PLD might arise from the membrane-embedded position of the substrate as well as the interactions of the enzyme with activators such as phosphatidylinositide (PIP_2).[39] A membrane-embedded substrate cannot reorganize; therefore, the second phosphoryl transfer and subsequent dead-end product formation would not occur.

In vitro, the rate-determining step for the transformation to dead-end product is the substrate reorganization (**B-3** to **C-1**). The next highest energy transition state is the first phosphoryl transfer (**A-TS-3-4**). However, the migration of OR^1 and exchange with H_2O (from **A-4** to **B-1**) should be considered irreversible. Thus, the low energy basin actually exists between the transition state of hydrolysis (**B-TS-1-2**) in **submechanism B** and substrate reorganization (the reorientation of substrate between **B-3** to **C-1**). The computed free energy of substrate reorganization of 20.7 kcal mol^{-1} supports the persistence of the geometry observed in the 1V0Y X-ray crystal structure on the minutes time scale. The transition states for P−N bond reformation with an apical OR^2 (**C-TS-1-2**), as well as the condensation of HOR^2 (**C-TS-3-4**), have activation free energies that are lower than those of the *in vivo* catalytic mechanism. Once the effective free energy of activation of substrate reorganization is achieved, the supermolecule will not persist as a five coordinate intermediate (**C-2** or **C-3**), but will instead quickly come to a resting state as the ″dead-end″ four-coordinate phosphohistidine product (1V0W/1V0V). Furthermore, experimental evidence for a ″dead-end″ four-coordinate phosphohistidine product in another PLD superfamily member (tyrosyl-DNA phosphodiesterase I, Tdp1) has recently been reported.[41] In Tdp1, the rate of substrate−enzyme association has been reported to be rate limiting.[42]

■ CONCLUSIONS

The *in vivo* catalytic activity of PLD_{PMF} can be divided into two submechanisms. The first *in vivo* submechanism (**A**) corresponds to the formation of the five-coordinate phosphohistidine intermediate and first phosphoryl transfer where the choline-like headgroup is cleaved. The second *in vivo* submechanism (**B**) corresponds to the hydrolysis of the phosphohistidine intermediate and bond dissociation of hydrolyzed substrate. A third submechanism (**C**) corresponds to the *in vitro* formation of a four-coordinate phosphohistidine intermediate that is very thermodynamically stable and kinetically favorable. The lowest-energy pathway for each of the three submechanisms has been mapped and discussed in unsurpassed atomic-level detail. The structural similarities between the geometries of **B-2** and **C-4** and the known PLD_{PMF} X-ray crystal structures (1V0Y and 1V0W/1V0V/1V0T/1V0U, respectively) are quite striking.

After extensive searches, not one three-coordinate metaphosphate minimum was located, nor were any transition states found that contain phosphorane character. *However, five-coordinate phosphorane intermediates were located.* These structural details support an associative mechanism for each phosphoryl transfer in each submechanism, not dissociative or interchange mechanisms. This study provides bountiful computational evidence in line with the experimental observation of a five coordinate phosphorane intermediate in 1V0Y. The catalytic activity of PLD_{PMF} and perhaps all members of the phospholipase D superfamily proceed via associative phosphoryl transfers.

Our computations indicate that formation and cleavage of the PN_{170} bond are both thermodynamically and kinetically facile (**A-TS-1-2** and **B-TS-2-3**). The first phosphoryl transfer (**A-TS-3-4**) is the *in vivo* rate-limiting step of the activated PLD_{PMF} enzyme. Based on computed dissociation energies of the substrate when implicit solvation effects are considered, the time-scale (minutes to hours) of substrate elimination is competitive with *in vitro/in silico* substrate reorganization, resulting in formation of the four-coordinate phosphohistidine ″dead-end″ product, which is a thermodynamic sink. The relatively small size and enhanced solubility of diC_4PC compared to typical *in vivo* phospholipids, as well as the artificially high concentration utilized in the crystallization conditions are the main factors attributed to the surprising ″PLC-like″/promiscuous activity of PLD_{PMF}. *In vivo*, membrane immobilization of the phospholipids dominates the kinetics because PLD ″scoots″ after formation of PA and release of choline. The immobilized substrate will not ″reorganize″ before PLD ″scoots″.

The HKD motif is highly conserved in the PLD superfamily. Therefore, quantitative mechanistic insight of PLD_{PMF} should be transferable to many other superfamily members. Findings from this article, as well as ongoing theoretical work being carried out in our laboratory, support the associative-type mechanism for phosphoryl transfers within the PLD superfamily. Tyrosyl-DNA phosphodiesterase I has also recently been reported to form a ″dead-end″ four-coordinate phosphohistidine product. Further experimental evidence for other members of this superfamily exhibiting PLC activity/behaving promiscuously under similar *in vitro* conditions would be quite interesting.

■ ASSOCIATED CONTENT

Supporting Information

Full citations for reference 21, 2D representations of each submechanism, a table containing total and relative energies of each species, and coordinates of optimized species. This material is available free of charge via the Internet at http://pubs.acs.org.

■ AUTHOR INFORMATION

Corresponding Author

*E-mail: cewebstr@memphis.edu

Author Contributions

All authors have given approval to the final version of the manuscript.

Notes

The authors declare no competing financial interest.

■ ACKNOWLEDGMENTS

We thank the University of Memphis High Performance Computing Facility and Computational Research on Materials Institute (CROMIUM) for computing support. This work was supported by the National Science Foundation (CAREER) CHE 0955723 and the University of Memphis.

■ REFERENCES

(1) Selvy, P. E.; Lavieri, R. R.; Lindsley, C. W.; Brown, H. A. *Chem. Rev.* **2011**, *111*, 6064−6119.
(2) (a) De Maria, L.; Vind, J.; Oxenboll, K. M.; Svendsen, A.; Patkar, S. *Appl. Microbiol. Biotechnol.* **2007**, *74*, 290−300. (b) Buxmann, W.; Bindrich, U.; Heinz, V.; Knorr, D.; Franke, K. *Colloids Surf., B* **2010**, *76*, 186−191.
(3) Ulbrich-Hofmann, R.; Lerchner, A.; Oblozinsky, M.; Bezakova, L. *Biotechnol. Lett.* **2005**, *27*, 535−544.
(4) Benson, D. A.; Karsch-Mizrachi, I.; Lipman, D. J.; Ostell, J.; Sayers, E. W. *Nucleic Acids Res.* **2010**, *38*, D46−D51.
(5) Exton, J. H. *Rev. Physiol., Biochem. Pharmacol.* **2002**, *144*, 1−94.
(6) Hanahan, D. J.; Chaikoff, I. L. *J. Biol. Chem.* **1947**, *168*, 233−240.
(7) Saito, M.; Kanfer, J. *Arch. Biochem. Biophys.* **1975**, *169*, 318−323.
(8) Kater, L. A.; Goetzl, E. J.; Austen, K. F. *J. Clin. Invest.* **1976**, *57*, 1173−1180.
(9) (a) Hammond, S. M.; Altshuller, Y. M.; Sung, T.-C.; Rudge, S. A.; Rose, K.; Engebrecht, J.; Morris, A. J.; Frohman, M. A. *J. Biol. Chem.* **1995**, *270*, 29640−29643. (b) Ponting, C. P.; Kerr, I. D. *Protein Sci.* **1996**, *5*, 914−922. (c) Secundo, F.; Carrea, G.; D'Arrigo, P.; Servi, S. *Biochemistry* **1996**, *35*, 9631−9636. (d) Sung, T. C.; Roper, R. L.; Zhang, Y.; Rudge, S. A.; Temel, R.; Hammond, S. M.; Morris, A. J.; Moss, B.; Engebrecht, J.; Frohman, M. A. *EMBO J.* **1997**, *16*, 4519−4530.
(10) Koonin, E. V. *Trends Biochem. Sci.* **1996**, *21*, 242−243.
(11) Stuckey, J. A.; Dixon, J. E. *Nat. Struct. Biol.* **1999**, *6*, 278−284.
(12) Gottlin, E. B.; Rudolph, A. E.; Zhao, Y.; Matthews, H. R.; Dixon, J. E. *Proc. Natl. Acad. Sci. U.S.A.* **1998**, *95*, 9202−9207.
(13) Abousalham, A.; Riviere, M.; Teissere, M.; Verger, R. *Biochim. Biophys. Acta* **1993**, *1158*, 1−7. Yang, S. F.; Freer, S.; Benson, A. A. *J. Biol. Chem.* **1967**, *242*, 477−484.
(14) Leiros, I.; Hough, E.; D'Arrigo, P.; Carrea, G.; Pedrocchi-Fantoni, G.; Secundo, F.; Servi, S. *Acta Crystallogr., Sect. D: Biol. Crystallogr.* **2000**, *56*, 466−468.
(15) Leiros, I.; Secundo, F.; Zambonelli, C.; Servi, S.; Hough, E. *Struct. Fold. Des.* **2000**, *8*, 655−667.
(16) Leiros, I.; McSweeney, S.; Hough, E. *J. Mol. Biol.* **2004**, *339*, 805−820.
(17) (a) Benkovic, S. J.; Schray, K. J. In *Transition States of Biochemical Processes*; Gandour, R. D., Schowen, R. L., Eds.; Plenum Press: New York, 1978; pp 493−527. (b) Knowles, J. R. *Annu. Rev. Biochem.* **1980**, *49*, 877−919. (c) Marcos, E.; Crehuet, R.; Anglada, J. M. *J. Chem. Theory Comput.* **2008**, *4*, 49−63. (d) Mercero, J. M.; Barrett, P.; Lam, C. W.; Fowler, J. E.; Ugalde, J. M.; Pedersen, L. G. *J. Comput. Chem.* **2000**, *21*, 43−51. (e) Orth, E. S.; Brandão, T. A. S.; Souza, B. S.; Pliego, J. R.; Vaz, B. G.; Eberlin, M. N.; Kirby, A. J.; Nome, F. *J. Am. Chem. Soc.* **2010**, *132*, 8513−8523. (f) Re, S. Y.; Imai, T.; Jung, J.; Ten-No, S.; Sugita, Y. *J. Comput. Chem.* **2011**, *32*, 260−270. (g) Swamy, K. C. K.; Kumar, N. S. *Acc. Chem. Res.* **2006**, *39*, 324−333. (h) Wilkie, J.; Gani, D. *J. Chem. Soc., Perkin Trans. 2* **1996**, 783−787. (i) Fersht, A. *Structure and Mechanism in Protein Science: A Guide to Enzyme Catalysis and Protein Folding*; W. H. Freeman and Co.: New York, 1999. (j) Lahiri, S. D.; Zhang, G. F.; Dunaway-Mariano, D.; Allen, K. N. *Science* **2003**, *299*, 2067−2071. (k) Tremblay, L. W.; Zhang, G. F.; Dai, J. Y.; Dunaway-Mariano, D.; Allen, K. N. *J. Am. Chem. Soc.* **2005**, *127*, 5298−5299. (l) Baxter, N. J.; Blackburn, G. M.; Marston, J. P.; Hounslow, A. M.; Cliff, M. J.; Bermel, W.; Williams, N. H.; Hollfelder, F.; Wemmer, D. E.; Waltho, J. P. *J. Am. Chem. Soc.* **2008**, *130*, 3952−3958. (m) Baxter, N. J.; Olguin, L. F.; Golicnik, M.; Feng, G.; Hounslow, A. M.; Bermel, W.; Blackburn, G. M.; Hollfelder, F.; Waltho, J. P.; Williams, N. H. *Proc. Natl. Acad. Sci. U.S.A.* **2006**, *103*, 14732−14737. (n) Marcos, E.; Field, M. J.; Crehuet, R. *Proteins: Struct. Funct. Bioinf.* **2010**, *78*, 2405−2411. (o) Frey, P. A.; Hegeman, A. D. *Enzymatic Reaction Mechanisms*; Oxford University Press: Oxford, U.K., 2007. (p) Jencks, W. P. *Catalysis in Chemistry and Enzymology*; Dover: New York, 1987. (q) Westheimer, F. H. *Science* **1987**, *235*, 1173−1178. (r) Cho, H.; Wang, W. R.; Kim, R.; Yokota, H.; Damo, S.; Kim, S. H.; Wemmer, D.; Kustu, S.; Yan, D. L. *Proc. Natl. Acad. Sci.* **2001**, *98*, 8525−8530. (s) Admiraal, S. J.; Herschlag, D. *J. Am. Chem. Soc.* **2000**, *122*, 2145−2148. (t) Lassila, J. K.; Zalatan, J. G.; Herschlag, D. *Annu. Rev. Biochem.* **2011**, *80*, 669−702. (u) Wong, K. Y.; Gu, H.; Zhang, S. M.; Piccirilli, J. A.; Harris, M. E.; York, D. M. *Angew. Chem. Int. Ed.* **2012**, *51*, 647−651. (v) Kamerlin, S. C. L.; Sharma, P. K.; Prasad, R. B.; Warshel, A. *Q. Rev. Biophys.* **2013**, *46*, 1−132. (w) Klahn, M.; Rosta, E.; Warshel, A. *J. Am. Chem. Soc.* **2006**, *128*, 15310−15323. (x) Kamerlin, S. C. L.; Haranczyk, M.; Warshel, A. *ChemPhysChem* **2009**, *10*, 1125−1134. (y) Hengge, A. C. *Biochim. Biophys. Acta, Proteins Proteomics* **2013**, *1834*, 415−416. (z) Cleland, W. W.; Hengge, A. C. *Chem. Rev.* **2006**, *106*, 3252−3278. (aa) Cleland, W. W.; Hengge, A. C. *FASEB J.* **1995**, *9*, 1585−1594. (bb) Cliff, M. J.; Bowler, M. W.; Varga, A.; Marston, J. P.; Szabo, J.; Hounslow, A. M.; Baxter, N. J.; Blackburn, G. M.; Vas, M.; Waltho, J. P. *J. Am. Chem. Soc.* **2010**, *132*, 6507−6516. (cc) Golicnik, M.; Olguin, L. F.; Feng, G. Q.; Baxter, N. J.; Waltho, J. P.; Williams, N. H.; Hollfelder, F. *J. Am. Chem. Soc.* **2009**, *131*, 1575−1588. (dd) Baxter, N. J.; Bowler, M. W.; Alizadeh, T.; Cliff, M. J.; Hounslow, A. M.; Wu, B.; Berkowitz, D. B.; Williams, N. H.; Blackburn, G. M.; Waltho, J. P. *Proc. Natl. Acad. Sci.* **2010**, *107*, 4555−4560. (ee) Bigley, A. N.; Raushel, F. M. *Biochim. Biophys. Acta, Proteins Proteomics* **2013**, *1834*, 443−453. (ff) Allen, K. N.; Dunaway-Mariano, D. *Trends Biochem. Sci.* **2004**, *29*, 495−503. (gg) Holmes, R. R. *Acc. Chem. Res.* **2004**, *37*, 746−753. (hh) Prasad, B. R.; Plotnikov, N. V.; Warshel, A. *J. Phys. Chem. B* **2013**, *117*, 153−163. (ii) Gu, H.; Zhang, S.; Wong, K.-Y.; Radak, B. K.; Dissanayake, T.; Kellerman, D. L.; Dai, Q.; Miyagi, M.; Anderson, V. E.; York, D. M.; Piccirilli, J. A.; Harris, M. E. *Proc. Natl. Acad. Sci.* **2013**, *110*, 13002−13007.
(18) Webster, C. E. *J. Am. Chem. Soc.* **2004**, *126*, 6840−6841.
(19) Waite, M. *Biochim. Biophys. Acta, Mol. Cell. Biol. Lipids* **1999**, *1439*, 187−197. Uesugi, Y.; Hatanaka, T. *Biochim. Biophys. Acta, Mol. Cell. Biol. Lipids* **2009**, *1791*, 962−969.
(20) (a) Siegbahn, P. E. M.; Crabtree, R. H. *J. Am. Chem. Soc.* **1997**, *119*, 3103−3113. (b) Zampella, G.; Kravitz, J. Y.; Webster, C. E.; Fantucci, P.; Hall, M. B.; Carlson, H. A.; Pecoraro, V. L.; De Gioia, L. *Inorg. Chem.* **2004**, *43*, 4127−4136. (c) Himo, F.; Siegbahn, P. E. M. *Chem. Rev.* **2003**, *103*, 2421−2456. (d) Siegbahn, P. E. M.; Borowski, T. *Faraday Discuss.* **2011**, *148*, 109−117. (e) Siegbahn, P. E. M.; Himo, F. *J. Biol. Inorg. Chem.* **2009**, *14*, 643−651. (f) Siegbahn, P. E. M.; Himo, F. *Wiley Interdiscip. Rev. Comput. Mol. Sci.* **2011**, *1*, 323−336. (g) Griffin, J. L.; Bowler, M. W.; Baxter, N. J.; Leigh, K. N.; Dannatt, H. R. W.; Hounslow, A. M.; Blackburn, G. M.; Webster, C. E.; Cliff, M. J.; Waltho, J. P. *Proc. Natl. Acad. Sci. U.S.A.* **2012**, *109*, 6910−6915.
(21) Frisch, M. J.; Trucks, G. W.; Schlegel, H. B. et al. Gaussian 09, Revision C. 01; Gaussian, Inc.; Wallingford, CT, 2009.
(22) Dapprich, S.; Komaromi, I.; Byun, K. S.; Morokuma, K.; Frisch, M. J. *J. Mol. Struct. THEOCHEM* **1999**, *461*, 1−21.
(23) (a) Becke, A. D. *J. Chem. Phys.* **1993**, *98*, 5648−5652. (b) Lee, C. T.; Yang, W. T.; Parr, R. G. *Phys. Rev. B: Condens. Matter* **1988**, *37*, 785−789.
(24) (a) Petersson, G. A.; Al-Laham, M. A. *J. Chem. Phys.* **1991**, *94*, 6081−6090. (b) Hariharan, P. C.; Pople, J. A. *Theor. Chim. Acta* **1973**, *28*, 213−222.
(25) Foresman, J. B.; and Frisch, Æ., *Exploring Chemistry with Electronic Structure Methods*, 2nd ed.; Gaussian, Inc.: Pittsburgh, PA; p 110.
(26) Stewart, J. J. P. *J. Mol. Model.* **2007**, *13*, 1173−1213.
(27) Ogino, C.; Daido, H.; Ohmura, Y.; Takada, N.; Itou, Y.; Kondo, A.; Fukuda, H.; Shimizu, N. *Biochim. Biophys. Acta, Proteins Proteomics* **2007**, *1774*, 671−678.

(28) Carrea, G.; D'Arrigo, P.; Piergianni, V.; Roncaglio, S.; Secundo, F.; Servi, S. *Biochim. Biophys. Acta, Lipids Lipid Metab.* **1995**, *1255*, 273−279.
(29) Barone, V.; Cossi, M. *J. Phys. Chem. A* **1998**, *102*, 1995−2001.
(30) Noodleman, L.; Lovell, T.; Han, W. G.; Li, J.; Himo, F. *Chem. Rev.* **2004**, *104*, 459−508.
(31) A table of ONIOM QM:QM electronic energies [$E_{e(\mathrm{ONIOM\ QM:QM\ gas})}$] and ZPE-corrected energies [$E_{o(\mathrm{ONIOM\ QM:QM\ gas})}$], ONIOM QM:QM gas-phase free energies and relative free energies [$\Delta G^{\circ/\ddagger}{}_{(\mathrm{ONIOM\ QM:QM\ gas})}$], ONIOM QM:QM solution-phase free energies and relative free energies [$\Delta G^{\circ/\ddagger}{}_{(\mathrm{ONIOM\ QM:QM\ soln})}$], fully QM gas-phase electronic energies and relative electronic energies [$\Delta E_{e(\mathrm{QM//ONIOM\ QM:QM\ gas})}$], and fully QM solution-phase energies and relative solution-phase energies [$\Delta G^{\circ/\ddagger}{}_{(\mathrm{QM//ONIOM\ QM:QM\ soln})}$] for each step in the complete mechanism is given in Supporting Information.
(32) Hatanaka, T.; Negishi, T.; Mori, K. *Biochim. Biophys. Acta, Proteins Proteomics* **2004**, *1696*, 75−82.
(33) Jain, M. K.; Berg, O. G. *Biochim. Biophys. Acta* **1989**, *1002*, 127−156.
(34) Berg, O. G.; Gelb, M. H.; Tsai, M. D.; Jain, M. K. *Chem. Rev.* **2001**, *101*, 2613−2653.
(35) (a) Melo, E.; Martins, J. *Biophys. Chem.* **2006**, *123*, 77−94. (b) Mouritsen, O. G.; Andresen, T. L.; Halperin, A.; Hansen, P. L.; Jakobsen, A. F.; Jensen, U. B.; Jensen, M. Ø.; Jørgensen, K.; Kaasgaard, T.; Leidy, C.; Simonsen, A. C.; Peters, G. H.; Weiss, M. *J. Phys.: Condens. Matter* **2006**, *18*, S1293−S1304. (c) Singh, J.; Ranganathan, R.; Hajdu, J. *J. Phys. Chem. B* **2008**, *112*, 16741−16751. (d) Wagner, K.; Brezesinski, G. *Curr. Opin. Colloid Interface Sci.* **2008**, *13*, 47−53.
(36) In our larger ONIOM QM:QM models, we did find some higher-energy phosphoryl-transfer transition states that initially might appear to be ″concerted″ because they easily ″fell″ to four-coordinate phosphorus reactant/product (of the submechanisms). These transition states had higher free energies of activation than those reported of the ″lowest energy pathway″ of our reported submechanisms (by 2−14 kcal mol^{-1}). Furthermore, upon detailed analysis of the intrinsic reaction coordinates (IRCs) of these transition states, in every case, we located a converged stationary point that represents a five-coordinate intermediate on the (very soft) potential energy surface.
(37) IUPAC. *Compendium of Chemical Terminology*, 2nd ed. (the ″Gold Book″); compiled by McNaught, A. D., Wilkinson, A.; Blackwell Scientific Publications: Oxford, 1997. XML on-line corrected version: http://goldbook.iupac.org (2006) created by M. Nic, J. Jirat, B. Kosata; updates compiled by A. Jenkins. ISBN 0-9678550-9-8. doi:10.1351/goldbook; Accessed Mar 2013.
(38) Sometimes, following the imaginary vibrational mode of a transition state uncovers extra intermediates between the transition state and the connected local minima. These intermediates are identifiable (for example **A-2**); occasionally, these intermediates have small spurious imaginary frequencies. However, locating the transition states (for example **A-TS-2-3**) between these intermediates and the next minimum is exceptionally difficult. These transition states necessarily exist along the potential energy surface (ref 17i). These intermediary transition states are not the rate-limiting steps, nor do they qualitatively affect the profile of the proposed mechanism. Our inability to locate these transition states is more of an indication that they possess extremely low relative free energies of activation, rather than some previously unknown issue with the geometry optimization algorithms implemented in the *Gaussian09* software package.
(39) Mansfeld, J.; Ulbrich-Hofmann, R. *Biochim. Biophys. Acta, Mol. Cell. Biol. Lipids* **2009**, *1791*, 913−926.
(40) Aikens, C. L.; Laederach, A.; Reilly, P. J. *Proteins: Struct. Funct. Bioinf.* **2004**, *57*, 27−35.
(41) Gajewski, S.; Comeaux, E. Q.; Jafari, N.; Bharatham, N.; Bashford, D.; White, S. W.; van Waardenburg, R. C. A. M. *J. Mol. Biol.* **2012**, *416*, 725−725.
(42) Raymond, A. C.; Rideout, M. C.; Staker, B.; Hjerrild, K.; Burgin, A. B. *J. Mol. Biol.* **2004**, *338*, 895−906.